Boundary-Layer Meteorol (2012) 142:223–243
DOI 10.1007/s10546-011-9678-1

ARTICLE

Large-Eddy Simulation of Inhomogeneous Canopy Flows Using High Resolution Terrestrial Laser Scanning Data

Fabian Schlegel · Jörg Stiller · Anne Bienert · Hans-Gerd Maas · Ronald Queck · Christian Bernhofer

Received: 8 April 2011 / Accepted: 14 November 2011 / Published online: 2 December 2011

Abstract The effect of sub-tree forest heterogeneity in the flow past a clearing is investigated by means of large-eddy simulation (LES). For this purpose, a detailed representation of the canopy has been acquired by terrestrial laser scanning for a patch of approximately 190 m length in the field site "Tharandter Wald", near the city of Dresden, Germany. The scanning data are used to produce a high resolution plant area distribution (PAD) that is averaged over approximately one tree height (30 m) along the transverse direction, in order to simplify the LES study. Despite the smoothing involved with this procedure, the resulting two-dimensional PAD maintains a rich vertical and horizontal structure. For the LES study, the PAD is embedded in a larger domain covered with an idealized, horizontally homogeneous canopy. Simulations are performed for neutral conditions and compared to a LES with homogeneous PAD and recent field measurements. The results reveal a considerable influence of small-scale plant distribution on the mean velocity field as well as on turbulence data. Particularly near the edges of the clearing, where canopy structure is highly variable, usage of a realistic PAD appears to be crucial for capturing the local flow structure. Inside the forest, local variations in plant density induce a complex pattern of upward and downward motions, which remain visible in the mean flow and make it difficult to identify the "adjustment zone" behind the windward edge of the clearing.

Keywords Edge flow · Forest canopy · Heterogeneous vegetation · Large-eddy simulation · Terrestrial laser scanning · Turbulence

F. Schlegel (✉) · J. Stiller
Institute of Fluid Mechanics, Technische Universität Dresden, 01062 Dresden, Germany
e-mail: fabian.schlegel@tu-dresden.de

A. Bienert · H.-G. Maas
Institute of Photogrammetry and Remote Sensing, Technische Universität Dresden, 01062 Dresden, Germany

R. Queck · C. Bernhofer
Institute of Hydrology and Meteorology, Technische Universität Dresden, 01062 Dresden, Germany

1 Introduction

Understanding the interaction between plant canopies and the atmospheric boundary layer is of considerable interest for a broad range of applications including meteorology, agriculture, forestry and biology. In particular, the turbulent exchange of momentum, mass and energy has been the focus of research over several decades. For a general overview about this topic we refer to the surveys of Raupach and Thom (1981), Finnigan (2000), and de Langre (2008).

The ramified structure and random distribution of plants pose a notorious problem to the modelling of canopy flows: In field studies, heterogeneity is omnipresent and complicates the interpretation of measurements, whereas consideration of detailed plant morphology remains far beyond the reach of numerical studies. Notable exceptions are the investigation of isolated trees (Endalew et al. 2009, 2011), fractal plant models (Chester and Meneveau 2007), or arrays of simple, crop-like structures (e.g. Yue et al. 2007; Dupont et al. 2010).

Under certain conditions, e.g. within uniform stands, the canopy can be considered horizontally homogeneous and isotropic. Further common simplifications involve the neglect of structural diversity, flexibility and elasticity of plant parts. With these assumptions it is possible to characterize the canopy by a so-called plant or leaf area density (PAD or LAD) depending on the vertical direction only. Vertical integration yields an even more condensed measure, the plant or leaf area index (PAI or LAI), respectively. In addition, a drag coefficient is introduced for relating the PAD to the flow resistance caused by the vegetation.

The flow above and within such (quasi) homogeneous canopies has been investigated extensively in various field studies, laboratory experiments and numerical simulations (Shaw and Schumann 1992; Shaw and Patton 2003) that have added insight into the fundamental transport mechanisms. Noticing the strong inflection in the mean velocity profile, Raupach et al. (1996) established a relation to the mixing layer between two co-flowing streams. Using this analogy they were able to explain important features of canopy flows as a consequence of coherent eddies emerging from shear-layer instabilities. Recently, Finnigan et al. (2009) analyzed the turbulent canopy flow based on a large-eddy simulation (LES) and revealed dual-hairpin eddies as the principal structures that are associated with the observed ejection and sweep events.

In practice, uniform canopies are, of course, rather the exception than the rule. At the microscale, canopy variability results from the transition between forested and grassy patches as well as from plant diversity and distribution inside the stands themselves. As the flow over a forest edge can be viewed as a generic model for the first type of heterogeneity, various studies place a focus on it (e.g. Raynor 1971; Gash 1986; Irvine et al. 1997; Lee 2000; Belcher et al. 2003; Yang et al. 2006a,b; Detto et al. 2008; Sogachev et al. 2008; Cassiani et al. 2008; Dupont and Brunet 2008, 2009; Dupont et al. 2011). In most of these investigations vegetation was assumed to be horizontally homogeneous, although the influence of forest morphology has been addressed by several authors. Using LES, Cassiani et al. (2008) showed that the formation of recirculation zones in the interior and at the leeside edge is promoted by an increasing PAI, i.e., denser canopies. In spite of transverse homogeneity, flow separation occurred intermittently at different locations along the edge. Dupont and Brunet (2008) studied via LES the effect of a varying leaf area index and leaf area distribution in the flow across a windward edge. They found that the faster flow adjustment with a denser canopy is accompanied by a stronger flow distortion and gustiness in the near-edge zone. Edges that are characterized by a large and sparse trunk space tend to develop a sustained sub-canopy jet, a feature investigated later in more detail by in situ and numerical experiments (Dupont et al. 2011). Dupont and Brunet (2009) investigated the effect of edge shape on the tree stability by means of LES, and found that tree vulnerability is slightly

reduced downwind from tapered, sparse and small edges and enhanced downwind from dense ones.

To our knowledge, Bohrer et al. (2009) presented the first and so far only numerical study considering the aerodynamic effect of vertical and *horizontal* heterogeneities down to scales matching the crown size. The canopy data were produced with the virtual canopy generator V-CaGe, developed by Bohrer et al. (2007). V-CaGe generates virtual three-dimensional (3D) canopies based on patch maps and spatial autocorrelations of the observed properties. Using this functionality different scenarios (winter vs. spring, heterogeneous vs. patchy) were studied by means of LES and compared with corresponding field data. The simulations indicated that heterogeneity decreases the displacement height and increases the roughness length and penetration depth to be used in regional models. On the smaller scale, the heterogeneity pattern influences the spatial distribution of ejection and sweep events. As a result, so-called ejection and sweep hot spots develop, which can affect local gas exchange and particle transport significantly (Bohrer et al. 2008).

Bohrer et al. (2009) also mention the possibility of explicitly measuring the PAD and further canopy information using aerial and satellite photography, lidar and tree sampling. However, this alternative was regarded as too costly and therefore not pursued by them. On the other hand, photogrammetry has seen a rapid development over the last few years and is now regularly applied in forest inventory (see, e.g., Aschoff and Spiecker 2004; Maas et al. 2008; Vosselman and Maas 2010). Airborne and especially terrestrial laser scanning allow for largely automated acquisition of vegetation data with an unprecedented resolution down to decimetres or even less. Complemented by appropriate postprocessing methods these techniques produce three-dimensional distributions of the plant area density and further attributes, which reproduce forest morphology in a realistic way. Our objective is to take a first step in combining the promising opportunities of laser scanning with the potential of LES and to explore viability of this approach as a tool for investigating the flow over heterogeneous forest stands at sub-tree resolution. This paper presents the results of a preliminary study dealing with a small clearing inside a forested area near the city of Dresden, Germany. The field site, data acquisition by terrestrial laser scanning and measurement techniques are summarized in Sect. 2. To assess the benefits of using a more realistic plant representation, we performed two LES studies: one with a patch-wise homogeneous PAD, and another one with a PAD obtained from terrestrial laser scanning. The numerical model is described in Sect. 3. Section 4 provides a discussion of the computed velocity fields and turbulent statistics, including a comparison to the field data recorded at four measurement towers. Finally, the conclusions are presented in Sect. 5.

2 Field Study

2.1 Description of the Field Site

The subject of our investigation is a clearing located in the forest "Tharandter Wald" about 25 km south-west of the city of Dresden in Germany (50°57′49″N, 13°34′01″E and 380 m a.g.l.). The site accommodates an anchor station operated by the Institute of Hydrology and Meteorology of TU Dresden since 1958, which has been used in various European projects, e.g. EuroFlux (Bernhofer et al. 2003) and CarboEurope IP (Gruenwald and Bernhofer 2007). Therefore a large amount of meteorological, hydrological, ecological and remote sensing observations are available. Here we give only a brief overview (for more details see Feigenwinter et al. 2004; Gruenwald and Bernhofer 2007). The site consists of a forest stand

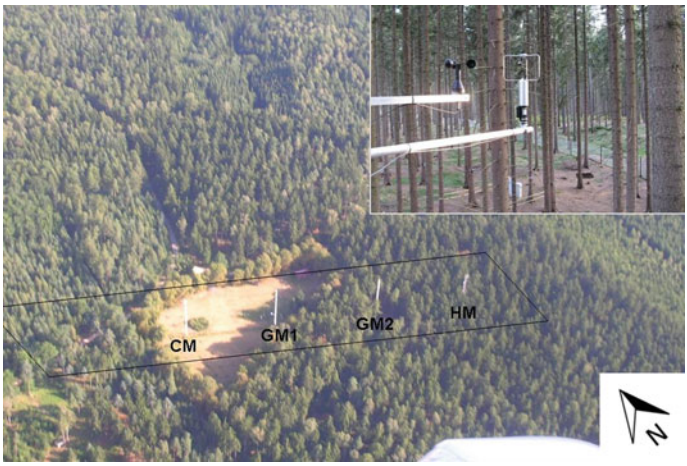

Fig. 1 Aerial photo with towers (courtesy of W. Junkermann, 31 July 2008) and the outlined investigation area (Queck et al. 2011). The small picture in the *upper right corner* shows the south-west view from a 42-m high permanent scaffolding tower at a height of 8 m

seeded in 1887 and a clearing of about 50 m × 90 m, named "Wildacker". The main canopy is composed of 87% coniferous evergreen (72% *Picea abies*, 15% *Pinus sylvestris*) and 13% deciduous (10% *Larix decidua*, 1% *Betula* species and 2% others) around the clearing. The stand is characterized by a dense canopy and an open trunk space with sparse understory (patches of replanted *Fagus sylvatica* as well as few *Sambucus* and *Sorbus aucuparia*). Grasses (mostly *Deschampsia flexuosa*) cover approximately 50% of the ground within the stand. The clearing is surrounded by a belt of chestnuts (*Castanea*) that smoothes the forest edge and closes the trunk space. The stand parameters are mainly based on an assessment in 1999. After thinning in 2002 the tree density is estimated to be about 335 trees per hectare and the single-sided PAD of about 7.1 $m^2\,m^{-2}$. The mean canopy height is about 35 m and the mean breast height diameter about 0.36 m. The investigated domain, marked by the frame in Fig. 1, is aligned according to the predominant wind direction of west to east and includes the clearing Wildacker.

In summer 2008, one permanent and three temporarily constructed measurement towers were used during a measurement campain. The permanent scaffolding tower (HM) stands 100 m east of the clearing inside a nearly homogeneous forest area and has a height of 42 m. Two temporarily constructed scaffolding towers (GM1 and GM2) of 40 m height were positioned in front and right behind the eastward forest edge. The remaining 30 m high telescoping tower (CM) was constructed at the opposite side of the clearing.

2.2 Terrestrial Laser Scanning

Laser scanning is an efficient three-dimensional measurement technique that is being used in an increasing range of application fields, including the acquisition of forest inventory parameters (see e.g., Vosselman and Maas 2010). For the present study two different terrestrial laser scanners were used to access the investigation area on a calm day. The scanning procedure is described in Bienert et al. (2010). In total, scans from 13 different ground positions and from the top of the permanent scaffolding tower HM were taken. The additional scans from the top of the tower are of great benefit for precisely recording the canopy without occlusions

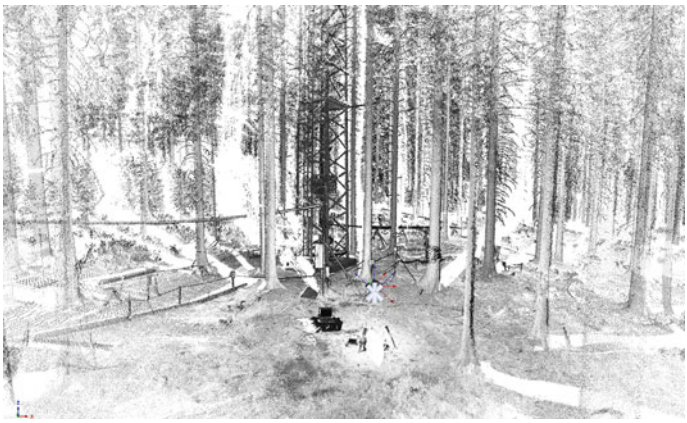

Fig. 2 Three-dimensional distribution of points representing the stand (thinned for printing purpose)

(see Queck et al. 2011). The average angular scan resolution was 0.1°, which results in a point spacing of 17 mm on an object at 10 m distance. To allow for an analysis of all point clouds in a common coordinate system, a geometric registration of all scans has to be performed. The scan registration was performed in an automatic manner using a distance pattern of identified tie points (see Bienert and Maas 2009). The stand is represented by approximately 50×10^6 points. Figure 2 shows part of a point distribution from the bottom of the tower HM.

In the next step the unorganized point distribution is converted into a voxel[1] representation. This is accomplished using a ray tracing method, which allows for identifying voxels that are penetrated by laser pulses before hitting an object. Based on the number of hits, penetrations and occlusions a reflection property is calculated for each voxel. The minimum voxel size is limited by the density and precision of the data points. State-of-the-art terrestrial laser scanners allow a voxel size of less than 0.1 m, which is far beyond the needs of the present study. Therefore, with respect to the minimum mesh size used in the numerical simulations, a voxel size of 1 m was chosen. As an example, Fig. 3 provides a comparison of the data points and the corresponding voxels of a spruce inside the stand.

The PAD, which is required in the numerical model, results from the reflection property by the application of a plant specific clumping factor (see Ryu et al. 2010). To determine this factor, which is unknown for laser measurements, the sum of the reflection properties within a small area of 30 m × 30 m around the tower HM is compared to a known PAI of 7.1 $m^2\ m^{-2}$ obtained from a forest assessment of six harvested Norway spruces. The resulting clumping factor is applied to the reflection property of all voxels (for more details see Queck et al. 2011).

2.3 Field Observations

The study uses wind measurements from two experiments called WinCanop and TurbEFA. WinCanop was carried out from June 2007 to November 2007 and TurbEFA from May 2008 to May 2009. The aim of the preceding experiment WinCanop was to obtain high resolution profiles in the canopy to optimize the design of the main experiment TurbEFA.

[1] A voxel is the three-dimensional equivalent of a pixel, i.e., a rectangular volume element with its faces aligned parallel to the coordinate axis.

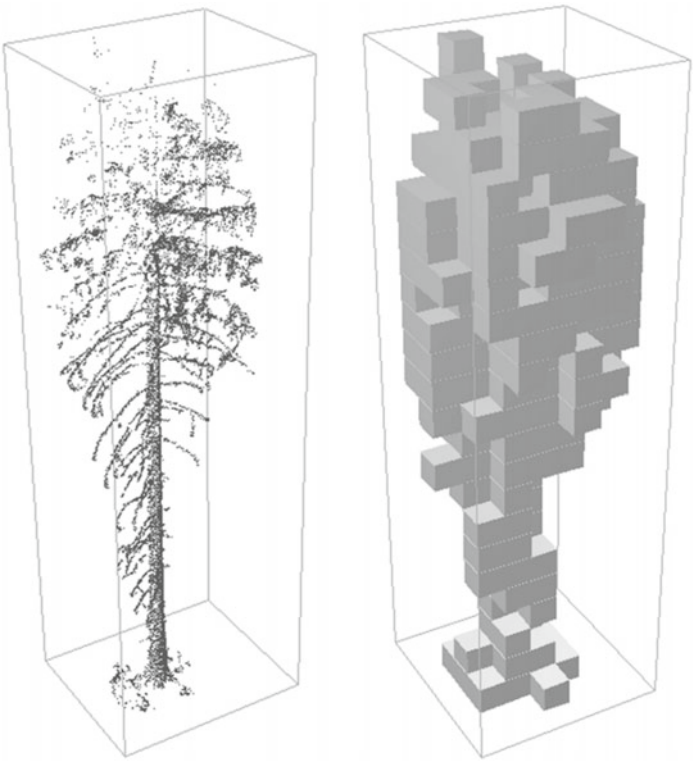

Fig. 3 Point cloud of a spruce (*left*) and occupied voxel space (voxel size 1 m) (*right*) with bounding box

The high frequency (20 Hz) samples of the wind vector were obtained by ultrasonic anemometers and thermometers ("sonics"). During WinCanop two comparison experiments took place to determine differences between the different sonics and sonic types. The set-up of WinCanop and the sonic comparison are documented in Queck and Bernhofer (2010).

In the framework of TurbEFA, turbulence measurements were performed at a transect over the clearing-forest interface. The set-up includes the four towers (up to 42 m) and five ground-level positions (2 m). In total 32 measurement positions were used to record the turbulent flow. A pattern of nineteen sensors was operated permanently at the four towers (at heights of 2, 10, 20, 30, and 40 m), and additionally 13 positions were temporarily operated by six rowing instruments to fill the gaps between the main positions (see Fig. 4).

We employed eighteen sonics of type Model 81000V (R.M. Young Meteorological Instruments, Michigan, USA) and seven sonics of type USA-1 (Metek GmbH, Germany). The sonics were mounted on booms at a distance of 2–3 m to the scaffolding towers and 1 m to the telescoping tower. The booms were orientated to the west to minimize the disturbance from the tower structure. Regular inspections of the sensors throughout the experiment ensured an accurate vertical and horizontal orientation.

Data from all the 25 sonics were recorded synchronously at 20 Hz. In postprocessing the raw data of the wind vector were rotated in one coordinate system and combined to produce 30-min statistics applying the software EdiRE (http://www.geos.ed.ac.uk/abs/research/micromet/EdiRe). Within these routines several quality tests were applied (i.e. tests of spikes, stationarity and data gaps). We applied limits for wind components ($\pm 30\,\mathrm{m\,s^{-1}}$) and sonic

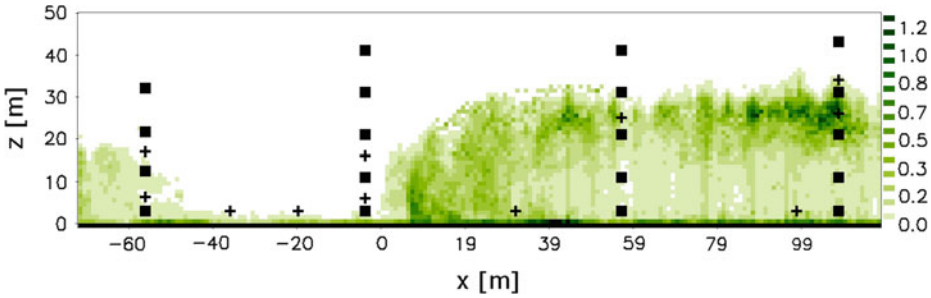

Fig. 4 Two-dimensional PAD in $\mathrm{m}^2\,\mathrm{m}^{-3}$, derived by averaging over the lateral direction. *Squares* indicate permanent and *crosses* temporary anemometer positions. The *square* at $x = 109\,\mathrm{m}$, $z = 42\,\mathrm{m}$ indicates a measurement and a reference anemometer. The *cross* at $x = 99\,\mathrm{m}$, $z = 2\,\mathrm{m}$ indicates two anemometers with different y locations (30 m distance)

temperature (-25 to $40\,^{\circ}\mathrm{C}$) on the 20-Hz data and excluded times with precipitation to avoid artefacts. In general, winds from the west (wind sector: 255–285 °, 12% of the time during the measurement campain) are investigated as this is the most prominent wind direction and is in line with the model domain and the tower set-up. In addition to these constraints, we restricted the investigated dataset to near-neutral cases, with the stability index $\zeta = z/L$, where L is the Obukhov length, ranging from -0.1 to 0.1 (based on measurements on tower HM at 42 m).

3 Numerical Method

3.1 Equations

Since we are interested mainly in the aerodynamic effects of small-scale plant distribution, we constrain our investigation to neutral atmospheric conditions and domains with dimensions of the order of 1 km. Therefore, variations in density and the influence of the Coriolis force can be neglected and, consequently, the flow is governed by the incompressible Navier–Stokes equations. Because the computational domain must be large enough to allow for an undisturbed evolution of the roughness sublayer and the coherent structures contained therein (Finnigan 2000), the grid resolution is typically confined to approximately 1 m, which leaves the smallest scales of motion unresolved. Within the LES approach, the resolved and the unresolved or subgrid scales (SGS) are formally separated from each other by using a filter operation (see, e.g., Sagaut 1998; Pope 2000). Application of the filter to the Navier–Stokes equations yields the resolved-scale or LES equations in the form

$$\partial_t \overline{u}_i + \partial_j \left(\overline{u}_j \overline{u}_i\right) = -\partial_i \overline{p} + \partial_j \left(2\nu \overline{S}_{ij}\right) + \partial_j \tau_{ij} + \overline{f}_{i,d} + \overline{f}_{i,p}, \tag{1}$$

$$\partial_i \overline{u}_i = 0, \tag{2}$$

where $\overline{\mathbf{u}}$, $\overline{p}$ are the resolved velocity and pressure, $\overline{S}_{ij} = \left(\partial_i \overline{u}_j + \partial_j \overline{u}_i\right)/2$ is the strain rate tensor and

$$\tau_{ij} = -\left(\overline{u_i u_j} - \overline{u}_i \overline{u}_j\right), \tag{3}$$

the so-called SGS stresses, which have to be modelled. Following the approach of Shaw and Schumann (1992) the plant drag results from the local wind speed $|\overline{\mathbf{u}}|$ and the PAD a augmented by an empirical drag coefficient c_d,

$$\overline{f}_{i,d} = -c_{\mathrm{d}} a \, |\overline{\mathbf{u}}| \, \overline{u}_i . \tag{4}$$

The last term in Eq. 1 represents the effect of the mesoscale pressure gradient that is imposed to maintain a prescribed bulk velocity under the presence of periodic boundary conditions.

To approximate the SGS stresses in Eq. 3 we use the one-equation model of Deardorff (1980) with the extensions to canopy flows introduced by Shaw and Schumann (1992). In our model the stresses are related to the resolved strain rate tensor by

$$\tau_{ij} = 2\nu_r \overline{S}_{ij} - \frac{2}{3}\delta_{ij}\overline{k''} \tag{5}$$

where

$$\nu_r = C_v \ell \overline{k''}^{1/2} \tag{6}$$

is the SGS viscosity, $\overline{k''} = \overline{u_i'' u_i''}/2$ is the unresolved turbulent kinetic energy (TKE) and $\ell = (\Delta x \, \Delta y \, \Delta z)^{1/3}$ is the SGS mixing length. Only the first term on the right-hand side of Eq. 5 is treated explicitly, whereas the second is merged into the resolved pressure $\overline{p}$. The model is closed by the SGS energy transport equation

$$\partial_t \overline{k''} + \partial_j \left(\overline{u}_j \overline{k''} \right) = \tau_{ij} \overline{S}_{ij} + \partial_j \left(2\nu_r \partial_j \overline{k''} \right) - C_E \frac{\overline{k''}^{3/2}}{\ell} - \frac{2\overline{k''}}{\tau} \tag{7}$$

where the last two terms model dissipation and the bypass effect associated with the enhanced breakdown of large structures in the canopy with time scale $\tau = \overline{u}_i / \overline{f}_{i,d}$. The model constants vary slightly in the literature, but their influence appears to be rather weak. Here we use the values according to Schmidt and Schumann (1989), i.e., $C_v = 0.0857$ and $C_E = 0.845$.

3.2 Discretization

The LES equations (1, 7) are discretized using a cell-centred finite volume method (Ferziger and Peric 1996) and implemented using the OpenFOAM® CFD toolbox 1.6. The method employs the total variation diminishing (TVD) fluxes of Sweby (1984) for convective terms and central differences for diffusive fluxes and SGS stresses. A backward differencing scheme of second-order accuracy in conjunction with the Pressure-Implicit with Splitting of Operators algorithm for enforcing continuity (Issa 1985) serves for time integration. In order to reduce the computational cost, the scheme involves an iterative procedure for evaluating the convective terms (see Jasak 1996). This technique limits the timestep to Courant numbers of 0.5, which is a rather mild restriction for LES. To reduce the simulation time of computations, OpenFOAM® takes advantage from parallelization by using a domain decomposition method together with the message passing interface. In our preliminary studies, the solver scaled with 99% efficiency on up to 200 cores on a SGI Altix 4700 high performance computing system for a channel flow with 2×10^6 grid cells. For details of the numerical method and implementation we refer to Weller et al. (1998).

For simulations of canopy flows the PAD can be prescribed analytically or as an attribute of the voxel representation. The PAD associated with a cell of the computational grid is then defined as the average over the covered region.

3.3 Model Evaluation

In order to evaluate the numerical model we considered the pioneering study of Shaw and Schumann (1992), who investigated the flow over and through a 20 m tall forest with $PAI = 2$ and a homogeneous PAD varying only in the vertical direction. The computational domain

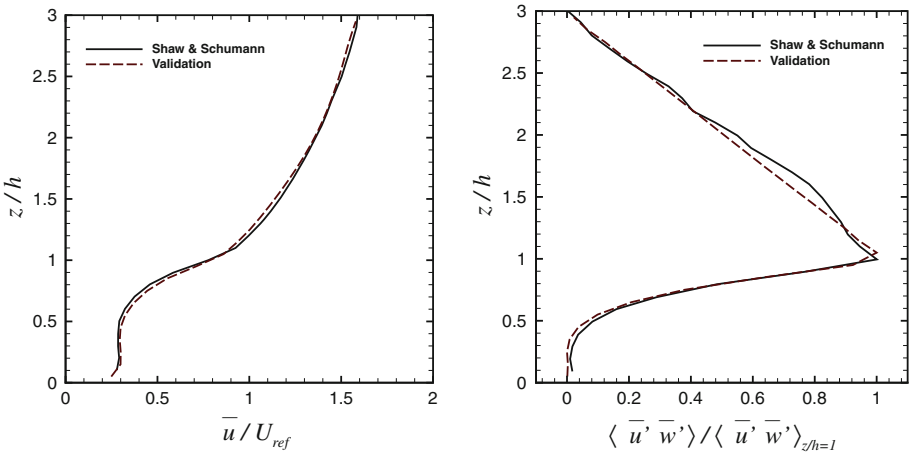

Fig. 5 Profiles of the mean velocity and the Reynolds stress of a homogeneous forest compared to the results of Shaw and Schumann (1992). The velocity is normalized by the vertically-averaged mean velocity and the Reynolds stress by the value at tree top

extends 192 m × 96 m × 60 m in streamwise, spanwise, and vertical directions and is discretized by an equidistant mesh with 2-m spacing. Taking advantage of homogeneity, periodicity is enforced in the first two (horizontal) directions, whereas no-slip condition is imposed at the bottom and free-slip at the top. Since the mesh spacing is too large for resolving the boundary layer, Shaw and Schumann (1992) employed the Obukhov wall function with a roughness length of $z_0 = 0.02$ m for computing the bottom shear stress. With neutral conditions the logarithmic law of the wall is recovered and, hence, used in our computations. The drag coefficient c_d is set to 0.15.

Figure 5 shows the computed mean velocity and the Reynolds stress along with the corresponding results of Shaw and Schumann (1992). It should be noticed that their data refer to weakly unstable conditions, since no plots were given for the neutral case. Despite this difference our results agree remarkably well with the reference data. A closer look at the Reynolds stress reveals a slightly weaker penetration of momentum into the canopy for neutral conditions, which is in close correspondence to the observations reported in Shaw and Schumann (1992). Above the canopy the Reynolds stress decays linearly to zero at the frictionless upper boundary, as required for steady state. The deviations in this region may be explained largely by the shorter averaging time used in the reference. A further effect is the upward shift of the peak Reynolds stress by one half of the mesh spacing due to the cell-centred variable arrangement in our method. Additional simulations showed that the peak moves exactly to tree-top height, if the latter is matched by a grid point.

4 Numerical Simulations

4.1 Overview

The intention of the present study is to investigate the feasibility of using laser scanning data for LES of canopy flows and to gain some insight into the effect of small-scale plant heterogeneity. In principle it would be possible to consider the fully three-dimensional PAD

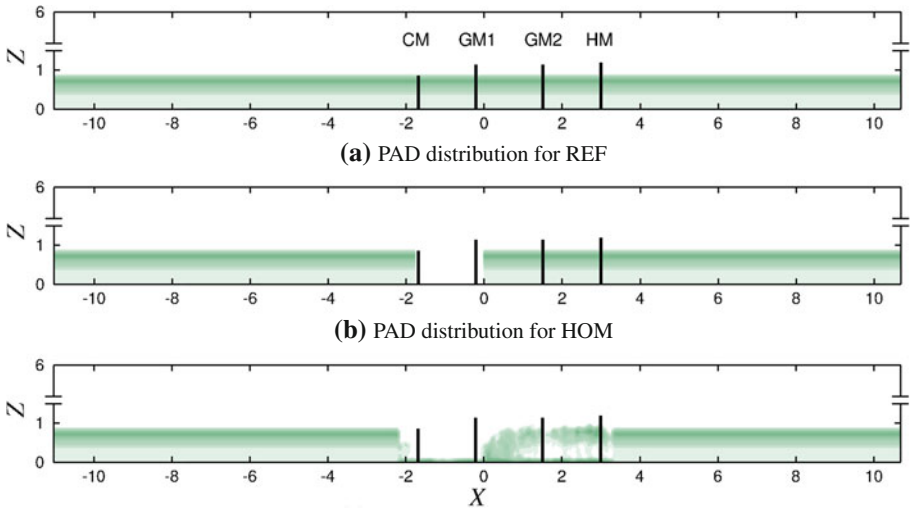

(a) PAD distribution for REF

(b) PAD distribution for HOM

(c) PAD distribution for HET

Fig. 6 Illustration of the used PAD distributions and the measurement tower positions in dimensionless coordinates according to Eq. 9. The tower CM is located at $-1.7h$, GM1 at $-0.2h$, GM2 at $1.5h$ and HM at $3h$

determined at the field site. However, since the terrestrial laser scanning postprocessing was restricted to a strip of 30-m width and 191-m length (including the clearing), we decided to use a simplified PAD, which represents the lateral average over the strip.

The computational domain is chosen as a compromise between the desired resolution and the dimensions that are necessary to accommodate the dominant coherent structures (Finnigan et al. 2009; Dupont and Brunet 2009) and to allow for flow adjustment behind the clearing (Yang et al. 2006a,b). It extends over 760 m $\times$ 380 m $\times$ 210 m in the streamwise, lateral and vertical directions, respectively. Given a mean canopy height of $h = 35$ m, this corresponds roughly to $22h \times 11h \times 6h$, which should be enough to meet the aforementioned requirements. In order to provide a reference state, we performed a LES for an infinite homogeneous canopy using the PAD determined at the permanent scaffolding tower (HM). This case is referred to as "REF". The second test case incorporates the clearing as a plant-free section that starts at $x = -60$ m and extends to $x = 0$, which yields a relative length of $l_c \approx 1.71h$. The forest stand is characterized by the same homogeneous PAD as for "REF", hence this case is referred to as "HOM". Finally, the third case, "HET", is defined by replacing the idealized PAD by the lateral average of the measured PAD in a section including a part of the leeside edge, the whole clearing and approximately 120 m of the adjacent, windward forest stand. Figure 6 shows the solution domains together with the different PAD distributions and the measurement towers.

All computations were performed using periodic boundary conditions in the streamwise and lateral directions, no-slip conditions at the bottom and free-slip at the top. For discretization we used a non-equidistant grid consisting of 220 $\times$ 190 $\times$ 82 cells with a spacing of 2 m in a sub-domain stretching from $x = -1.5h$ to $6.5h$ and $z \leq 4h$. Outside this region the streamwise and the vertical spacing were gradually increased to 6 m. To fit the measurement window of the field study, the mesoscale pressure forcing $\overline{f}_{x,p}$ was adjusted to achieve a mean velocity of approximately 4 m s^{-1} at a height of $z = 42$ m at tower HM.

Time integration was performed over a period of 10^4 s with a timestep of 0.025 s. Statistical moments were evaluated by averaging over the last 5000 s and, additionally, over the homogeneous (y) direction. Angle brackets indicate the mean value and a prime the fluctuations. In particular, the corresponding decomposition of velocity components is

$$\overline{u}_i = \langle \overline{u}_i \rangle + \overline{u}_i'. \tag{8}$$

For ease of analysis and to simplify notation we introduce the following dimensionless quantities:

– horizontal and vertical positions

$$X = x/h, \tag{9a}$$
$$Z = z/h. \tag{9b}$$

– velocity

$$U_i = \langle \overline{u}_i \rangle / U_{\text{ref}}, \tag{10a}$$
$$U_i' = \overline{u}_i' / U_{\text{ref}}, \tag{10b}$$

where U_{ref} represents the mean velocity recorded at tower HM at a height of $z = 42$ m. More specifically we denote the mean streamwise and vertical components as $U = U_1$ and $W = U_3$, respectively.

– streamfunction Ψ such that

$$\partial\Psi/\partial X = W, \tag{11a}$$
$$\partial\Psi/\partial Z = -U. \tag{11b}$$

Note that in the present case the lower boundary ($Z = 0$) represents a streamline (e.g. $\Psi = 0$) such that Ψ can be evaluated by means of vertical integration, i.e.,

$$\Psi(X, Z) = -\int_0^Z U\left(X, \tilde{Z}\right) \mathrm{d}\tilde{Z}. \tag{12}$$

– Reynolds shear stress

$$R_{xy} = -\left\langle U'W' \right\rangle, \tag{13}$$

– resolved turbulent kinetic energy

$$K = \left\langle U_i' U_i' \right\rangle / 2, \tag{14}$$

– skewness of the streamwise velocity

$$S_u = \left\langle U'^3 \right\rangle / \left\langle U'^2 \right\rangle^{3/2}. \tag{15}$$

4.2 Mean Velocity

To investigate the flow structure near the clearing the streamfunction as well as the streamwise and vertical velocity components are plotted in Figs. 7 and 8 for cases HOM and HET, respectively. In both cases the streamlines reveal a weak recirculation zone, which extends almost over the whole clearing (Figs. 7a, 8a). This result is consistent with the LES study

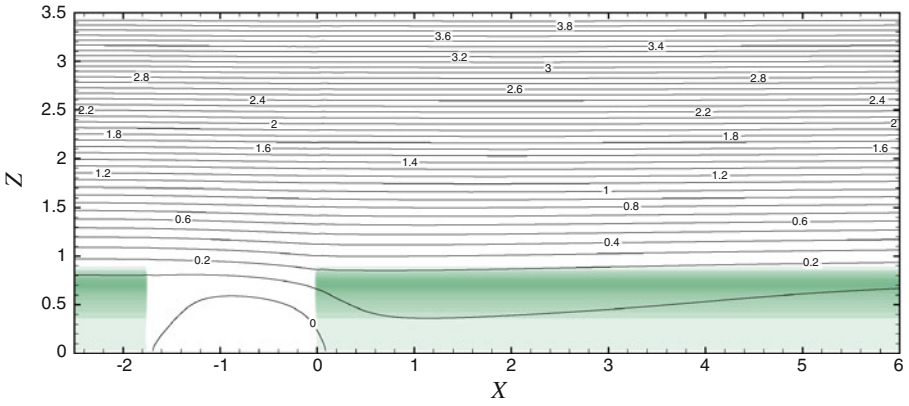

(a) Streamfunction Ψ

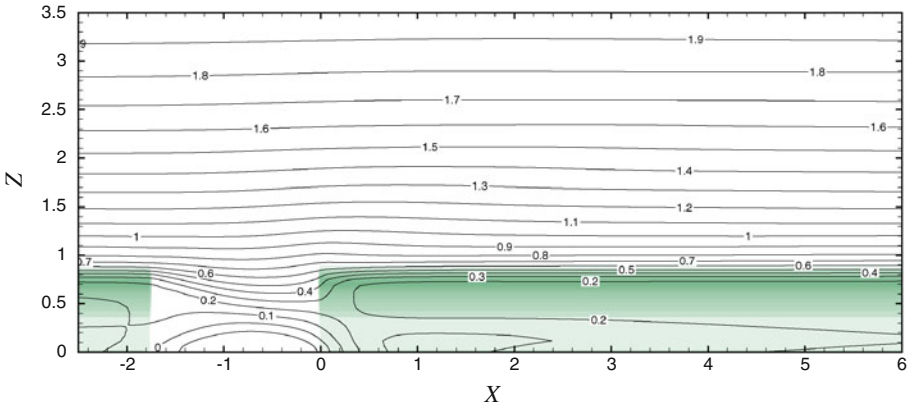

(b) Streamwise velocity U

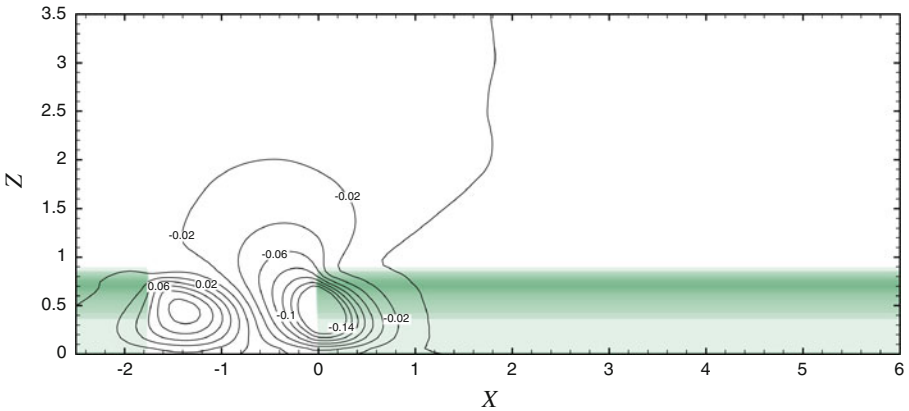

(c) Vertical velocity W

Fig. 7 Streamfunction and mean velocity distribution for case HOM. The coordinates and values are normalized according to Eqs. 9, 10 and 11. *Colouring* depicts the PAD

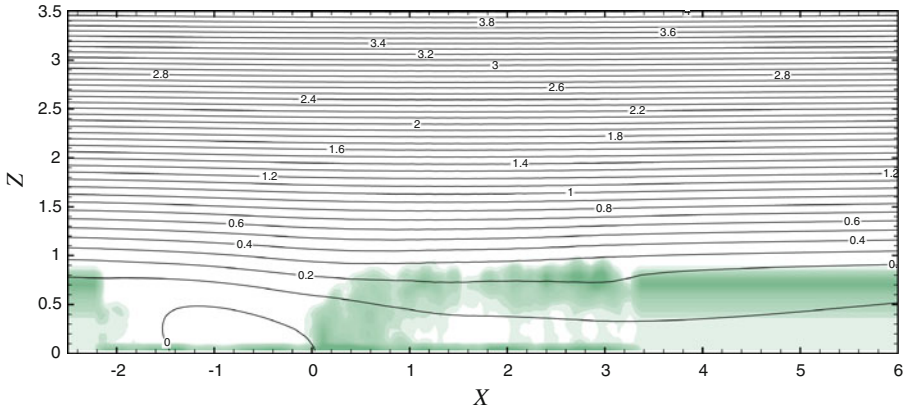

(a) Streamfunction Ψ

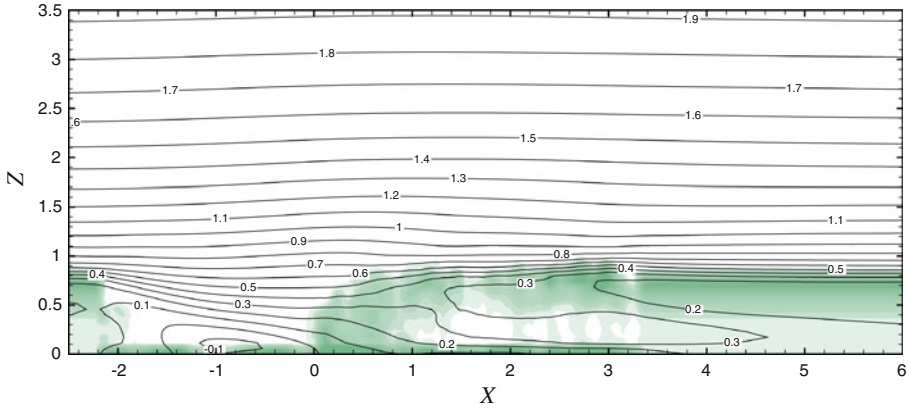

(b) Streamwise velocity U

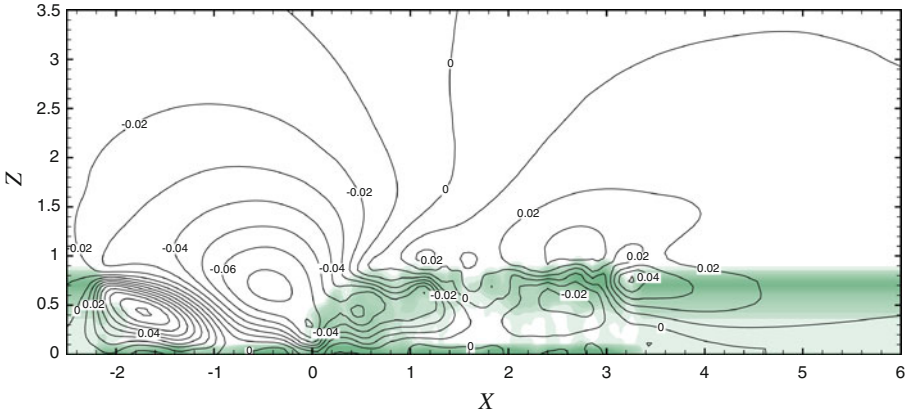

(c) Vertical velocity W

Fig. 8 Streamfunction and mean velocity distribution for case HET. The coordinates and values are normalized according to Eqs. 9, 10 and 11. *Colouring* depicts the PAD

of Cassiani et al. (2008), who observed the formation of a recirculation zone behind leeside forest edges for $LAI \geq 6$. In their investigations the flow reattached at approximately $3.4h$, which even exceeds the length of the present clearing. The presence of a recirculation zone in front of the windward forest edge leads to a flow pattern that differs qualitatively from the picture obtained for isolated edges or long clearings (e.g. Yang et al. 2006a; Dupont and Brunet 2009). Instead of being repelled, the flow penetrates the canopy from above in a short section adjacent to the edge. This feature is particularly well pronounced for the homogeneous canopy (Fig. 7c). However, a much longer distance is required for reaching equilibrium conditions: adopting the criterion of Dupont and Brunet (2008), $|W| < 0.01$ at $Z = 1$, the length of the adjustment zone is about $4.7h$ for case HOM. In case HET, the inclined slope and almost uniform PAD at the windward edge lead to more gently adaptation of the flow (Fig. 8a). This observation can be quantified in terms of the distortion angle that is formed between the mean flow vector and the horizontal direction at the location of highest wind speed in front of the edge. For the heterogeneous canopy the distortion angle is approximately 8°, as opposed to 41° for the homogeneous one. Apart from this detail, the course of streamlines and, hence, the flow topology resemble the latter case. Nonetheless a significant influence of the plant distribution is evident from the contour plots of the streamwise and vertical velocity components, Fig. 8b and c, respectively. While the streamwise velocity contours evolve a similar pattern as for the homogeneous stand for $x > 1.2$, the vertical component varies considerably within and above the heterogeneous patch. Except of the region very close to the edge these variations are closely linked with the small-scale heterogeneity of the PAD. Since the extremal values of W reach up to 3% of the reference velocity, one may expect that local changes in plant density give rise to a significant transport of mass and momentum through the canopy that cannot be captured with the assumption of a homogeneous PAD. As a further consequence it appears no longer adequate to define the adjustment zone in terms of vanishing vertical velocity.

Since the field site is characterized by a fine-grained, highly heterogeneous, three-dimensional vegetation, the influence of the actual plant distribution on the measurements is certainly not negligible. Figure 9 provides a comparison between computed and measured streamwise velocity at the tower positions, including the results of the reference simulation (REF) with continuous canopy. Tower CM stands close to the upwind edge of the clearing at $X = -1.7$. At this position, the streamwise velocity computed in case HOM differs only marginally from the reference, whereas the measurements reveal an increased magnitude, especially for $0.4 \leq Z \leq 0.7$. This discrepancy may be explained by the fact that the shape and the structure of the canopy are not well represented in the computation. Indeed, a slightly better agreement is achieved with case HET, where a realistic PAD is used for the outermost part of the edge. According to the findings of Cassiani et al. (2008) it may be argued that the assumption of a too dense canopy near the edge triggers the development of the recirculation zone observed in the LES studies, whereas the measurements at tower GM1 ($X = -0.2$) do not indicate any reverse flow (Fig. 9b). Again case HET shows a better agreement with the experimental data, which seems to support our hypothesis. The next tower, GM2, stands one and a half tree heights after the (nominal) position of the windward edge. Hence, the field data as well as the LES indicate a partial recovery of the asymptotic velocity profile obtained in the reference simulation (Fig. 9c). Case HOM fits nicely with the field data in the crown section, but develops a significant excess velocity in the trunk space. This deviation can be explained as a consequence of the idealized PAD, which fails to reproduce the natural canopy structure at the edge. In contrast, the streamwise velocity profile has the right shape in case HET, although the magnitude is overestimated in the trunk space. Further downstream, at tower HM ($X = 3$), both LES studies show a reasonable agreement with the field data for

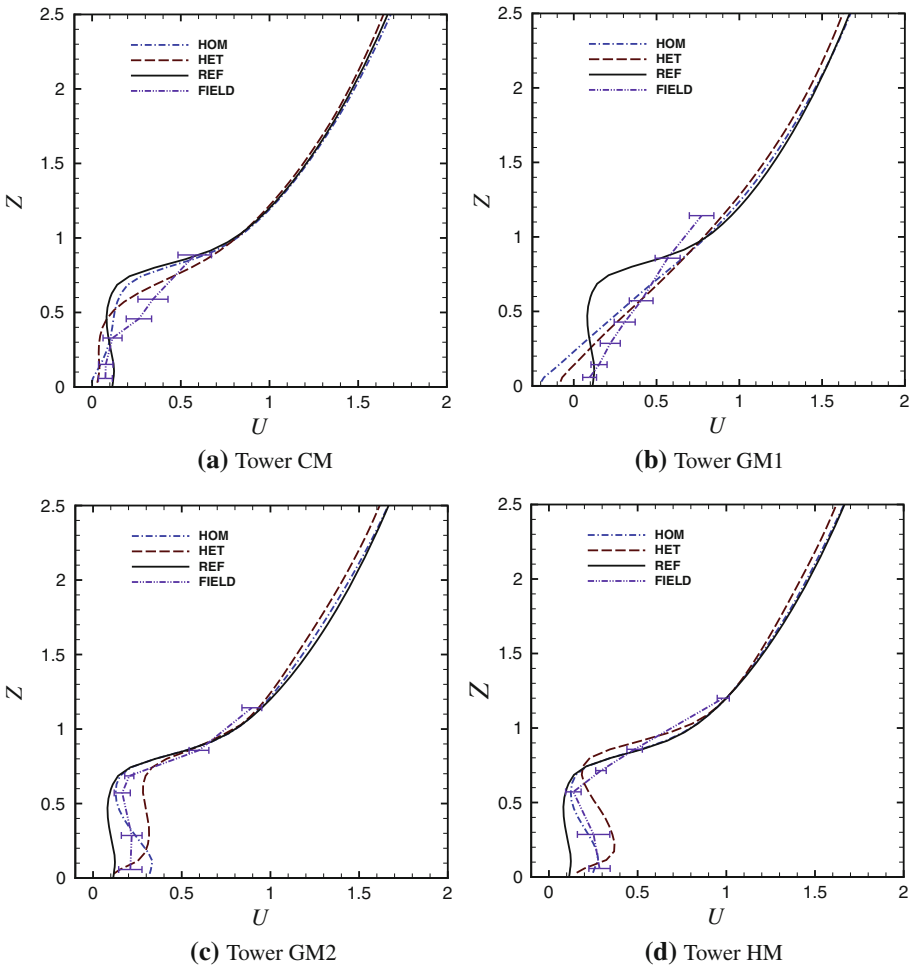

Fig. 9 Comparison of measured and computed normalized velocity profiles at the four measurement towers. The height is normalized by tree-height h and velocity according to Eq. 10. The tower positions are given in Fig. 6

U (Fig. 9d). Here HOM fits well to the measurements, whereas case HET again shows the tendency to overestimate the velocity magnitude in the trunk space.

4.3 Turbulence Statistics

Figures 10 and 11 depict the distributions of the mean turbulent energy K and the Reynolds stress R_{xz} for cases HOM and HET, respectively. In both cases, the turbulent fluctuations intensify in the shear layer separating the recirculation zone and the outer flow passing the clearing. The interaction between these regions reaches up to $Z \approx 2$ with the maximum TKE located approximately at $Z = 1.2$ just over the windward edge. For the homogeneous canopy we observe an intrusion of TKE into the trunk space, as reported previously, e.g., by Dupont et al. (2011). In contrast turbulence decays quickly while passing the denser and

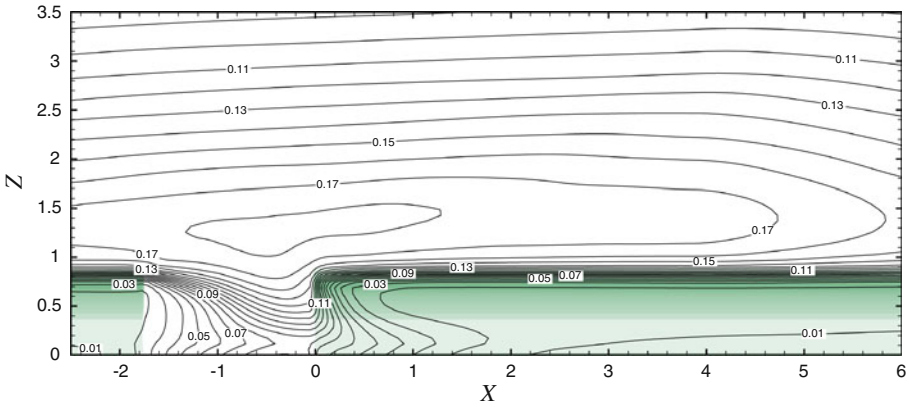

(a) Turbulent kinetic energy

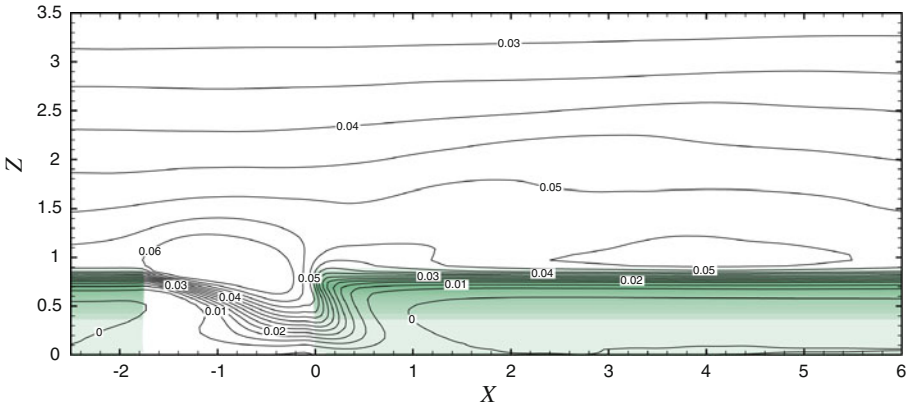

(b) Reynolds stress

Fig. 10 Turbulent energy and Reynolds stress for case HOM. The coordinates and values are normalized according to Eqs. 9, 13 and 14. *Colouring* depicts the PAD

largely closed edge in case HET (Fig. 11a). Generally, however, the effect of small-scale plant distribution is less visible as for the vertical velocity. Similar observations can be made for the Reynolds shear stress, which peaks at $Z \approx 1$ within the shear layer above the clearing. As with TKE, the Reynolds stress decays more rapidly within the trunk space immediately behind the edge in case HET due to the denser PAD. It is worth noting, however, that R_{xz} attains its maximum before the TKE, i.e., upstream of the latter. Obviously, this behaviour cannot be reproduced correctly by closures that model turbulent viscosity based on the mean TKE only.

Figure 12 provides a comparison between the measured and computed profiles of K and R_{xz} at the tower positions. For the turbulent energy, both LES studies, HOM and HET, fit well to the corresponding field data. At tower CM, close to the leeward edge, case HET achieves a better quantitative and qualitative agreement. This may be explained as a secondary effect of the more realistic PAD, which leads to a smaller recirculation zone than in case of the homogeneous canopy. As a consequence, turbulent energy from the upstream canopy top is transported downward after passing the edge, whereas the velocity and hence, the

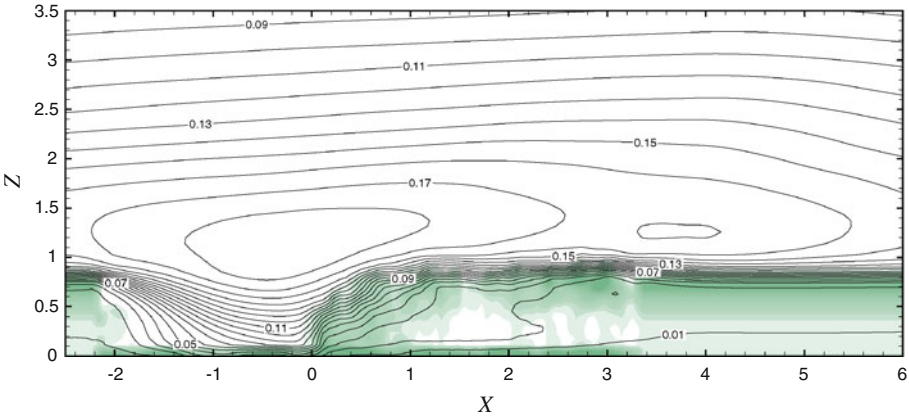

(a) Turbulent kinetic energy

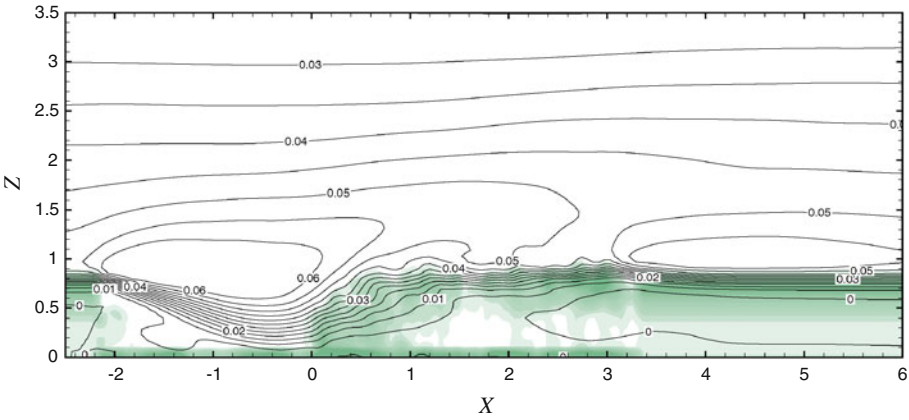

(b) Reynolds stress

Fig. 11 Turbulent energy and Reynolds stress for case HET. The coordinates and values are normalized according to Eqs. 9, 13 and 14. *Colouring* depicts the PAD

mean transport direction at $Z \approx 1$, remains virtually parallel to the ground in case HOM. Thus the TKE is enhanced for HET, while staying close to the asymptotic profile inside the continuous forest (REF) for case HOM.

The right-hand column of Fig. 12 shows the corresponding results for the Reynolds shear stress. Both LES studies failed to reproduce the profiles measured above the clearing (towers CM and GM1), whereas good agreement is achieved inside the stand (towers GM2 and HM). The disagreement at the first two towers is certainly related to the formation of a recirculation zone and hence a separated shear layer in the LES, which has no match in the field data. Inside the homogeneous canopy the shear-stress distribution soon adopts a shape similar to the reference simulation. It is characterized by a small positive momentum flux within a layer reaching from the bottom to the lower boundary of the crown section at $Z \approx 0.4$. The presence of an upward momentum flux near the edge was reported already in earlier work including wind-tunnel experiments (Morse et al. 2002), numerical studies (Sogachev et al. 2008) and in situ field measurements (Dupont et al. 2011). It is worth noting, however, that in the present case the field study as well as the LES case HET indicate a

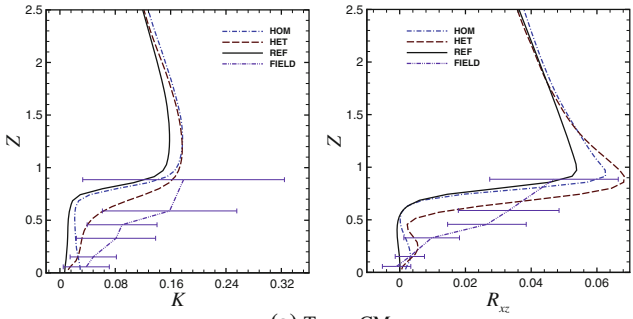

(a) Tower CM

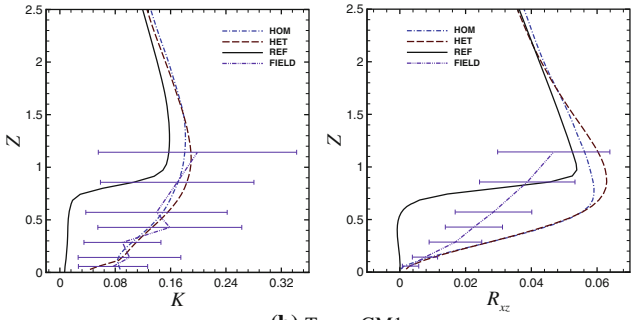

(b) Tower GM1

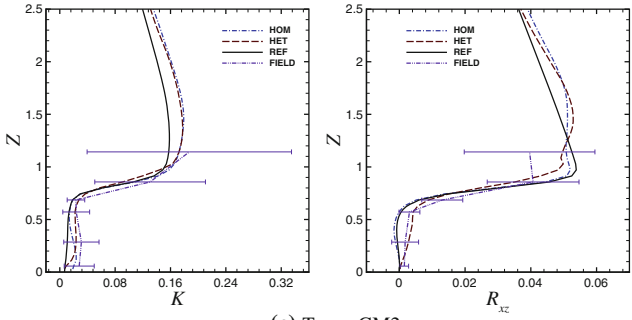

(c) Tower GM2

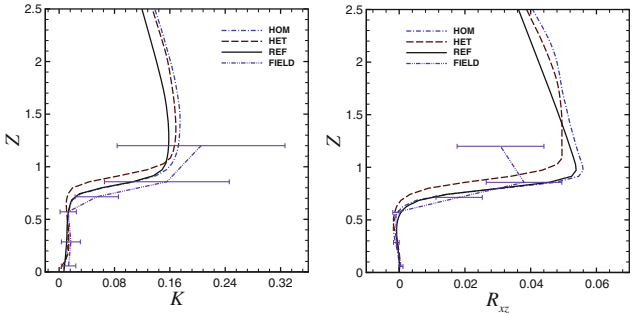

(d) Tower HM

Fig. 12 Comparison of measured and computed profiles of normalized turbulent kinetic energy and normalized Reynolds stress at the measurement towers. The normalization is according to Eqs. 9, 13 and 14. The tower positions are given in Fig. 6

Table 1 Normalized skewness of mean streamwise velocity fluctuations at tower HM ($X = 3$)

z (m)	Z	REF	HOM	HET	FIELD
2	0.057	−0.09	−0.03	−0.08	0.23
10	0.286	−0.06	−0.05	0.02	0.24
20	0.571	−0.05	−0.02	−0.07	0.23
30	0.857	1.15	1.05	0.55	0.79
42	1.200	0.36	0.24	0.30	0.24

delay in the development of the positive momentum-flux layer, which becomes visible only at tower HM.

To assess the existence of a possible enhanced gust zone, the skewness of streamwise velocity fluctuations was analyzed at tower HM (Table 1). In the reference simulation the skewness is slightly negative in trunk space and lower crown region, but increases up to 1.15 near the tree-top level, which fits well to earlier investigations (Raupach et al. 1996). For case HOM we obtained similar, though slightly smaller, magnitudes. Hence, there is no evidence for an enhanced gust zone, in contrast to observations made for free edges (Yang et al. 2006b; Dupont and Brunet 2008). For case HET we notice a reduction of the peak level of about 50% in comparison to HOM. This finding suggests that the influence of vegetation heterogeneity is stronger for the skewness than for the second-order moments. Finally, Table 1 also lists the corresponding field data. Contrary to the LES, the measured skewness remains positive throughout the trunk space, whereas the maximum is comparable in size and location.

5 Conclusions

The flow through and above a heterogeneous forest with a clearing was investigated by means of LES. For the first time, a high-resolution PAD distribution obtained from terrestrial laser scanning was used to model the aerodynamic drag caused by the vegetation. Despite the simplification introduced by lateral averaging of the measured PAD, the study revealed a significant influence of small-scale plant distribution on the mean velocity field as well as on the turbulence field. Particularly near the edges, where canopy structure is highly variable, the employment of a realistic PAD appears to be crucial for capturing the local flow structure, Reynolds shear stresses and transport of turbulent kinetic energy. Local variations in plant density generate a complex pattern of sustained up and downward motions inside and above the forest stand. This feature has no counterpart in the concurrent LES study that was performed with a homogeneous canopy. The induced velocity regularly exceeds 2% of the reference velocity U_{ref}. This is a magnitude comparable to the order of the turbulent fluctuations. As a consequence, the effect of small-scale heterogeneities needs to be considered for a proper evaluation of mass and momentum transport through canopies.

Notwithstanding its preliminary character, the present study strongly encourages the use of detailed vegetation data for LES of canopy flows. In the near future, terrestrial and airborne laser scanning will become available to acquire the necessary terrain and vegetation data for larger areas and, possibly in combination with a virtual canopy generator (Bohrer et al. 2007), allow for more realistic 3D studies.

Acknowledgments The work was supported by the German National Science Foundation (Deutsche Forschungsgemeinschaft, DFG) within the DFG priority programme 1276 MetStröm: Multiple Scales in Fluid Mechanics and Meteorology. Computational facilities were provided by the Centre for Information Services and High Performance Computing (ZIH) of the TU Dresden.

References

Aschoff T, Spiecker H (2004) Algorithms for the automatic detection of trees in laser scanner data. In: Int Arch Photogramm, Remote Sens Spat Inf Sci XXXVI-8/W2:71–75

Belcher S, Jerram N, Hunt J (2003) Adjustment of a turbulent boundary layer to a canopy of roughness elements. J Fluid Mech 488:369–398. doi:10.1017/S0022112003005019

Bernhofer C, Aubinet M, Clement R, Grelle A, Gruenwald T, Ibrom A, Jarvis P, Rebmann C, Schulze E, Tenhunen J (2003) Fluxes of carbon, water and energy of European forests. In: Ecological studies, vol 163, Springer, Chap Spruce forests (Norway and Sitka spruce, including Douglas fir): Carbon and water fluxes and balances, ecological and ecophysiological determinants, pp 99–123

Bienert A, Maas HG (2009) Methods for the automatic geometric registration of terrestrial laserscanner point clouds in forest stands. In: Int Arch Photogramm, Remote Sens Spat Inf Sci XXXVIII-3/W8:1–6

Bienert A, Queck R, Schmidt A, Bernhofer C, Maas HG (2010) Voxel space analysis of terrestrial laser scans in forests for wind field modelling. In: Int Arch Photogramm, Remote Sens Spat Inf Sci XXXVIII—Part 5:92–97

Bohrer G, Wolosin M, Brady R, Avissar R (2007) A virtual canopy generator (v-cage) for modelling complex heterogeneous forest canopies at high resolution. Tellus B 59:566–576. doi:10.1111/j.1600-0889.2007.00253.x

Bohrer G, Katul G, Nathan R, Walko R, Avissar R (2008) Effects of canopy heterogeneity, seed abscission and inertia on wind-driven dispersal kernels of tree seeds. J Ecol 96:569–580

Bohrer G, Katul G, Walko R, Avissar R (2009) Exploring the effects of microscale structural heterogeneity of forest canopies using large-eddy simulations. Boundary-Layer Meteorol 132:351–382

Cassiani M, Katul G, Albertson J (2008) The effects of canopy leaf area index on airflow across forest edges: large-eddy simulation and analytical results. Boundary-Layer Meteorol 126:433–460. doi:10.1007/s10546-007-9242-1

Chester S, Meneveau C (2007) Renormalized numerical simulation of flow over planar and non-planar fractal trees. Environ Fluid Mech 7:289–301. doi:10.1007/s10652-007-9026-7

de Langre E (2008) Effects of wind on plants. Annu Rev Fluid Mech 40:141–168. doi:10.1146/annurev.fluid.40.111406.102135

Deardorff J (1980) Stratocumulus-capped mixed layers derived from a three-dimensional model. Boundary-Layer Meteorol 18:495–527

Detto M, Katul G, Siqueira M, Juang JY, Stoy P (2008) The structure of turbulence near a tall forest edge: the backward-facing step flow analogy revisited. Ecol Appl 18:1420–1435

Dupont S, Brunet Y (2008) Edge flow and canopy structure: a large-eddy simulation study. Boundary-Layer Meteorol 126:51–71. doi:10.1007/s10546-007-9216-3

Dupont S, Brunet Y (2009) Coherent structures in canopy edge flow: a large-eddy simulation study. J Fluid Mech 630:93–128

Dupont S, Gosselin F, Py C, de Langre E, Hemon P, Brunet Y (2010) Modelling waving crops using large-eddy simulation: comparison with experiments and a linear stability analysis. J Fluid Mech 652:5–44. doi:10.1017/S0022112010000686

Dupont S, Bonnefond JM, Irvine M, Lamaud E, Brunet Y (2011) Long-distance edge effects in a pine forest with a deep and sparse trunk space: in situ and numerical experiments. Agric For Meteorol 151:328–344. doi:10.1016/j.agrformet.2010.11.007

Endalew A, Hertog M, Delele M, Baetens K, Persoons T, Baelmans M, Ramon H, Nicolai B, Verboven P (2009) Cfd modelling and wind tunnel validation of airflow through plant canopies using 3D canopy architecture. Int J Heat Fluid Flow 30:356–368. doi:10.1016/j.ijheatfluidflow.2008.12.007

Endalew A, Debaer C, Rutten N, Vercammen J, Delele M, Ramon H, Nicolaï B, Verboven P (2011) Modelling the effect of tree foliage on sprayer airflow in orchards. Boundary-Layer Meteorol 138:139–162. doi:10.1007/s10546-010-9544-6

Feigenwinter C, Bernhofer C, Vogt R (2004) The influence of advection on the short term CO_2—budget in and above a forest canopy. Boundary-Layer Meteorol 113:201–224

Ferziger J, Peric M (1996) Computational methods for fluid dynamics. Springer, Berlin

Finnigan J (2000) Turbulence in plant canopies. Annu Rev Fluid Mech 32:519–571

Finnigan J, Shaw R, Patton E (2009) Turbulence structure above a vegetation canopy. J Fluid Mech 637:387–424. doi:10.1017/S0022112009990589

Gash J (1986) Observations of turbulence downwind of a forest–heath interface. Boundary-Layer Meteorol 36:227–237

Gruenwald T, Bernhofer C (2007) A decade of carbon, water and energy flux measurements of an old spruce forest at the anchor station tharandt. Tellus B 59:387–396

Irvine M, Gardiner B, Hill M (1997) The evolution of turbulence across a forest edge. Boundary-Layer Meteorol 84:467–496

Issa I (1985) Solution of the implicitly discretised fluid flow equations by operator-splitting. J Comput Phys 62:40–65

Jasak H (1996) Error analysis and estimation for the finite volume method with applications to fluid flows. PhD thesis, Imperial College, London

Lee X (2000) Air motion within and above forest vegetation in non-ideal conditions. For Ecol Manag 135:3–18

Maas HG, Bienert A, Scheller S, Keane E (2008) Automatic forest inventory parameter determination from terrestrial laserscanner data. Int J Remote Sens 29(5):1579–1593. doi:10.1080/01431160701736406

Morse A, Gardiner B, Marshall B (2002) Mechanisms controlling turbulence development across a forest edge. Boundary-Layer Meteorol 103:227–251

Pope SB (2000) Turbulent flows. Cambridge University Press, Cambridge, 806 pp

Queck R, Bernhofer C (2010) Constructing wind profiles in forests from limited measurements of wind and vegetation structure. Agric For Meteorol 150:724–735. doi:10.1016/j.agrformet.2010.01.012

Queck R, Bienert A, Maas HG, Harmansa S, Goldberg V, Bernhofer C (2011) Wind fields in heterogeneous conifer canopies: parameterisation of momentum absorption using high-resolution 3D vegetation scans. Eur J For Res 1–12. doi:10.1007/s10342-011-0550-0

Raupach M, Thom A (1981) Turbulence in and above plant canopies. Annu Rev Fluid Mech 13:97–129

Raupach M, Finnigan J, Brunet Y (1996) Coherent eddies and turbulence in vegetation canopies: the mixing-layer analogy. Boundary-Layer Meteorol 78:351–382

Raynor G (1971) Wind and temperature structure in a coniferous forest and a contiguous field. For Sci 17: 351–363

Ryu Y, Nilson T, Kobayashi H, Sonnentag O, Law B, Baldocchi D (2010) On the correct estimation of effective leaf area index: does it reveal information on clumping effects? Agric For Meteorol 150:463–472. doi:10.1016/j.agrformet.2010.01.009

Sagaut P (1998) Large eddy simulation for incompressible flows. Springer, New York

Schmidt H, Schumann U (1989) Coherent structure of the convective boundary layer derived from large-eddy simulations. J Fluid Mech 200:511–562

Shaw R, Patton E (2003) Canopy element influences on resolved- and subgrid-scale energy within a large-eddy simulation. Agric For Meteorol 115:5–17

Shaw R, Schumann U (1992) Large-eddy simulation of turbulent flow above and within a forest. Boundary-Layer Meteorol 61:47–64

Sogachev A, Leclerc M, Zhang G, Rannik Ů, Vesala T (2008) CO_2 fluxes near a forest edge: a numerical study. Ecol Appl 16(6):1454–1469

Sweby P (1984) High resolution schemes using flux limiters for hyperbolic conservation laws. SIAM J Numer Anal 21(5):995–1011

Vosselman G, Maas HG (2010) Airborne and terrestrial laser scanning. Whittles Publishing, Dunbeath, 336 pp

Weller G, Tabor G, Jasak H, Fureby C (1998) A tensorial approach to computational continuum mechanics using object-oriented techniques. Comput Phys 12(6):620–631

Yang B, Morse A, Shaw R, Paw U KT (2006a) Large-eddy simulation of turbulent flow across a forest edge. Part II: Momentum and turbulent kinetic energy budgets. Boundary-Layer Meteorol 121:433–457. doi:10.1007/s10546-006-9083-3

Yang B, Raupach M, Shaw R, Paw U KT, Morse A (2006b) Large-eddy simulation of turbulent flow across a forest edge. Part I: Flow statistics. Boundary-Layer Meteorol 120:377–412. doi:10.1007/s10546-006-9057-5

Yue W, Parlange M, Meneveau C, Zhu W, van Hout R, Katz J (2007) Large-eddy simulation of plant canopy flows using plant-scale representation. Boundary-Layer Meteorol 124:183–203. doi:10.1007/s10546-007-9173-x